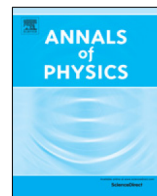




ELSEVIER

Contents lists available at ScienceDirect

Annals of Physics

journal homepage: www.elsevier.com/locate/aop

Bound states with orbital angular momentum in the continuum of cylindrical non-axisymmetric waveguide

A.A. Lyapina^{a,b}, A.S. Pilipchuk^{a,b}, A.F. Sadreev^{a,*}

^a Kirensky Institute of Physics, Academy of Sciences, 660036 Krasnoyarsk, Russia

^b Siberian Federal University, 660080, Krasnoyarsk, Russia

ARTICLE INFO

Article history:

Received 14 September 2016

Accepted 29 May 2018

Available online 5 July 2018

Keywords:

Acoustic wave transmission

Spinning trapped modes with orbital angular momentum

ABSTRACT

We consider acoustic wave transmission in a non-axisymmetric waveguide which consists of a cylindrical resonator of radius R and length L and two cylindrical waveguides of radius $r < R$ whose axes are shifted relative to the axis of the resonator and relative to each other by azimuthal angle $\Delta\phi$. We find multiple bound states in the continuum (trapped modes) with nonzero orbital angular momentum under variation of L due to full destructive interference of resonant modes leaking into waveguides. For $\Delta\phi = \pi/2$ we find the degenerate bound states in the continuum whose contribution into the scattering wave function is complex and supports giant vortical acoustic intensity spinning inside the resonator.

© 2018 Elsevier Inc. All rights reserved.

Considerable attention has recently been focused on bound states in the continuum (BIC) or the trapped modes in perturbed acoustic waveguides. Many different geometrical configurations with Neumann boundary conditions have been studied. These studies have shown that the existence of trapped modes is very sensitive to choice of geometry. Up to now geometrical configurations were chosen to reduce the effective dimension of the acoustic waveguide. Chronologically, the following specific perturbed acoustic waveguides were considered. In 1951 Urcell [1,2] considered a sphere placed on the axis of a cylindrical guide and shown that a trapped mode exists for selected radius of the sphere. Linton and McIver [3] proved the existence of an infinite number of trapped modes for the case of cylindrical waveguide containing an axisymmetric obstacle, in particular a thin circular sleeve.

Similarly, the dimension is reduced in acoustical waveguides of rectangular cross-section in yOz plane and directed along the x -axis with obstacle shaped only in the xOy plane so that the thickness

* Corresponding author.

E-mail address: almas@tnp.krasn.ru (A.F. Sadreev).

of the perturbed waveguide along the z -axis d is constant. Then the scattering channels are given by the eigenmodes quantized along the z -axis with corresponding Neumann boundary conditions at the walls positioned at $z = \pm d/2$. The utmost case of these structures is a two-dimensional acoustical waveguide formed by two infinite parallel lines at distance d containing a circle of radius $R < d$ [4] or multiple circles [5,6] positioned symmetrically between them. The trapped modes are antisymmetric about the centerline of the guide to determine them as the symmetry protected BICs. More sophisticated BICs of the same symmetry as the symmetry of the continuum were demonstrated recently in Refs. [7–9].

A different class is the fully three-dimensional systems. For example, in the case of non-axisymmetric obstacle inside the cylindrical waveguide Hein and Coch [10] numerically computed acoustic resonances and BICs by solving the eigenvalue problem. Here we consider similar non-axisymmetric waveguide but without an obstacle inside as shown in Fig. 1. The axisymmetric case shown in Fig. 1(a) preserves the orbital angular momentum (OAM) m because of the rotational symmetry around the central axis that effectively reduces the dimension of the waveguide to two. The BICs with $m = 0$ were shown to occur under variation of the length of the resonator [8] due to full destructive interference of resonant states [11]. An equivalent explication of the BICs is that under variation of the resonator length the eigenmodes ψ_1, ψ_2 of the same symmetry as the symmetry of propagating modes of the waveguides become degenerate. Then the coupling of the superposed state $a_1\psi_1 + a_2\psi_2$ with the continuum can be canceled by a proper choice of the superposition coefficients a_1 and a_2 [12].

One can similarly consider BICs with $m \neq 0$. As before these BICs occur due to the accidental degeneracy of the inner eigenmodes of the cylindrical resonator $\psi_{mn}(r, \phi, z) = J_m(\mu_{mn}r)e^{im\phi}\psi_l(z)$ and $\psi_{mn'l}(r, \phi, z) = J_m(\mu_{mn'l}r)e^{im\phi}\psi_l(z)$ under variation of the length. Because of the degeneracy of the eigenmodes relative to $\pm m$ the BIC turns out to be degenerate relative to $\pm m$ in the form

$$\psi_{BIC}^m(r, \phi, z) = [AJ_m(\mu_{mn}r)\psi_l(z) + BJ_m(\kappa_{mn'l}r)\psi_l(z)] \begin{cases} \cos m\phi \\ \sin m\phi \end{cases} \quad (1)$$

In this paper, we consider BICs with OAM in the cylindrical resonator with non-axisymmetrically attached cylindrical waveguides of semi-infinite length as shown in Fig. 1(b) and (c). The lack of rotational symmetry results in resonant excitation of eigenmodes with $m \neq 0$ even if zero OAM $m = 0$ mode is injected through the waveguide. Our primary goal is to consider BICs which can be complex

$$\psi_{BIC}(r, \phi, z) = \sum_{ml} A_m J_m(\kappa_{mn'l}r)\psi_l(z) \exp(im\phi) \quad (2)$$

where coefficients of superposition $|A_{mnl}| \neq |A_{-mnl}|$. Then the BIC can carry the vector of acoustic energy flux which will be referred to the acoustic intensity vector [13]

$$\vec{j} = \text{imag}(\psi^* \nabla \psi) = |\psi|^2 \nabla \arg(\psi) \quad (3)$$

spinning inside the resonator.

For analysis of the BICs we employ the coupled mode theory (CMT) adapted for the Neumann BC [14]. The approach allows us to analytically predict the eigenfrequencies of the BICs as well as their shape functions. We will demonstrate that our approach not only represents an alternative numerical technique for finding BICs but provides an efficient analytical tool for calculation of the BICs in the two-mode approximation for the case in Fig. 1(b) and the four-mode approximation for the case in Fig. 1(c).

1. Acoustic coupled mode theory for open cylindrical resonators

An unambiguous tool for analysis of BICs is the effective non Hermitian Hamiltonian derived for open acoustic resonators in Refs. [8,14]. It is a result of the Feshbach projection [15,16] of the total

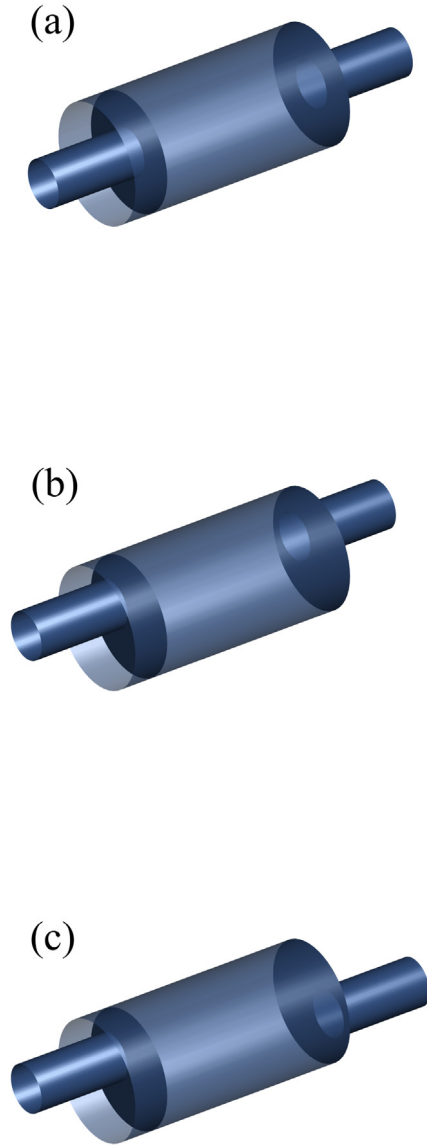


Fig. 1. Cylindrical resonator of radius R and length L with two attached cylindrical waveguides of radius $r < R$. The whole waveguide system is (a) axisymmetric, (b) non-axisymmetric with waveguides attached coaxially, and (c) non-axisymmetric with the waveguide axis misaligned by azimuthal angle difference $\Delta\phi = \pi/2$.

space resonator plus waveguides onto inner space of the resonator. The propagating modes in the hard cylindrical waveguides with Neumann boundary conditions are described by

$$\psi_{pq}(r, \phi, z) = \phi_{pq}(r) \frac{1}{2\pi \sqrt{k_{pq}}} \exp(ip\phi + ik_{pq}z), \quad (4)$$

$$\phi_{pq}(r) = \begin{cases} \frac{\sqrt{2}}{J_0(\mu_{0q})} J_0(\mu_{0q}r), & p = 0, \\ \sqrt{\frac{2}{\mu_{pq}^2 - p^2}} \frac{\mu_{pq}}{J_p(\mu_{pq})} J_p(\mu_{pq}r), & p = 1, 2, 3, \dots, \end{cases}$$

where r , are ϕ the polar coordinates in the xOy -plane, μ_{pq} is the q th root of equation

$$\left. \frac{dJ_p(\mu_{pq}r)}{dr} \right|_{r=1} = 0$$

imposed by the Neumann boundary condition on the walls of sound hard cylindrical waveguide.

$$k_{pq}^2 = \omega^2 - \mu_{pq}^2 \tag{5}$$

The dimensional quantities r , z , k_{pq} are measured in terms of the radius of the waveguide r and frequency is measured in the terms of the ratio s/R where s is the sound velocity. The propagating bands degenerate with the respect to the sign of OAM are classified by two indexes, the OAM index $p = 0, \pm 1, \pm 2, \dots$ and radial index $q = 1, 2, 3, \dots$. Profiles of propagating functions $\phi_{mq}(r) \cos p\phi$ and $\phi_{mq}(r) \sin p\phi$ are depicted in [Table 1](#). The inner Hilbert space of the closed cylindrical resonator is given by the following eigenmodes

$$\Psi_{mnl}(r, \phi, z) = \psi_{mn}(r) \sqrt{\frac{1}{2\pi}} \exp(im\phi) \psi_l(z), \tag{6}$$

where

$$\psi_{mn}(r) = \begin{cases} \frac{\sqrt{2}}{J_0(\mu_{0n}R)} J_0\left(\frac{\mu_{0n}r}{R}\right), & m = 0 \\ \sqrt{\frac{2}{\mu_{mn}^2 - m^2}} \frac{\mu_{mn}}{J_m(\mu_{mn}R)} J_m\left(\frac{\mu_{mn}r}{R}\right), & m = 1, 2, 3, \dots, \end{cases}$$

$$\psi_l(z) = \sqrt{\frac{2 - \delta_{l,1}}{L}} \cos[\pi(l - 1)z/L], \tag{7}$$

$l = 1, 2, 3, \dots$ and z is measured in terms of the waveguide radius. The corresponding eigenfrequencies are

$$\omega_{mnl}^2 = \left[\frac{\mu_{mn}^2}{R^2} + \frac{\pi(l - 1)^2}{L^2} \right] \tag{8}$$

where μ_{mn} is the n th root of the equation $\left. \frac{dJ_p(\mu_{mn}r)}{dr} \right|_{r=R} = 0$ which follows from the Neumann boundary condition on the walls of hard cylindrical waveguide.

Then the Feshbach projection of the total space of the open system onto the inner eigenmodes of the closed cylindrical resonator (6) gives us the following non Hermitian Hamiltonian [8,14]

$$\widehat{H}_{eff} = \widehat{H}_R - i \sum_{C=L,R} \sum_{pq} k_{pq} \widehat{W}_{C,pq} \widehat{W}_{C,pq}^+ \tag{9}$$








The matrix elements of \widehat{W} is given by overlapping integrals

$$W_{mnl;pq}^C = \psi_l(z = z_C) \int_0^{2\pi} d\phi' \int_0^1 r' dr' \psi_{pq}(r', \phi') \Psi_{mn}(r(r', \phi'), \phi(r', \phi')) \tag{10}$$

where $z_C = 0, L$ are the position of edges of the resonator along the z -axis. Hence according to Eq. (7) we have

$$\psi_l(0) = \sqrt{\frac{2 - \delta_{l,1}}{L}}, \psi_l(L) = \psi_l(0)(-1)^{l-1}.$$

Table 1
Cut-off frequencies and shapes of propagating modes.

Number of channel	Cut-off frequency	Indexes	Mode shape
1	0	$p = 0, q = 1$	
2	1.84118	$p = \pm 1, q = 1$	
3	3.0542	$p = \pm 2, q = 1$	
4	3.831706	$p = 0, q = 2$	
5	4.2012	$p = \pm 3, q = 1$	
6	5.3176	$p = \pm 4, q = 1$	
7	5.33145	$p = \pm 1, q = 2$	

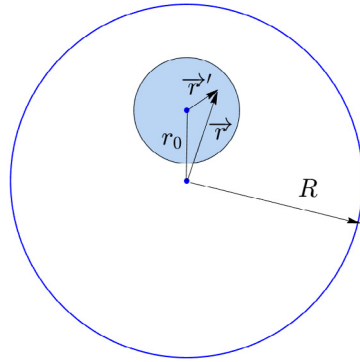


Fig. 2. Circles show cross-sections of waveguides with unit radius and resonator with radius R . Filled area shows integration area in Eq. (10).

Integration is performed over the cross section of the attached waveguides as shown in Fig. 2. According to Fig. 2 one can link the polar coordinates of the resonator and of the waveguide through the following equation

$$r \sin \phi = r_0 + r' \sin \phi', \quad r \cos \phi = r' \cos \phi'. \tag{11}$$

The formalism of the effective non Hermitian Hamiltonian forms a powerful basis for calculation of transmittance of sound waves through the resonator via the scattering matrix (S-matrix) [17,18]. Its matrix elements are given by the inversion of the matrix $\widehat{G} = (\widehat{H}_{eff} - \omega^2)^{-1}$, i.e., by the Green function

$$S_{pqC;p'q'C'} = -\delta_{C,C'} \delta_{p,p'} \delta_{q,q'} - 2ik_{pq} \sum_{mnl} W_{pq; mnl}^{C*} G_{mnl; m'n'l'} W_{m'n'l'; p'q'}^C. \tag{12}$$

When the waveguides are coaxially attached to the resonator as shown in Fig. 1(a) the azimuthal index is preserved to have $m = p$. The total Hilbert space and respectively the S-matrix is decomposed into the subspaces classified by m :

$$S_{qC;q'C'}^p = -\delta_{C,C'} \delta_{q,q'} - ik_{pq} \sum_{nl} W_{pq; nl}^{C*} G_{nl; n'l'}^p W_{n'l'; pq'}^C. \tag{13}$$

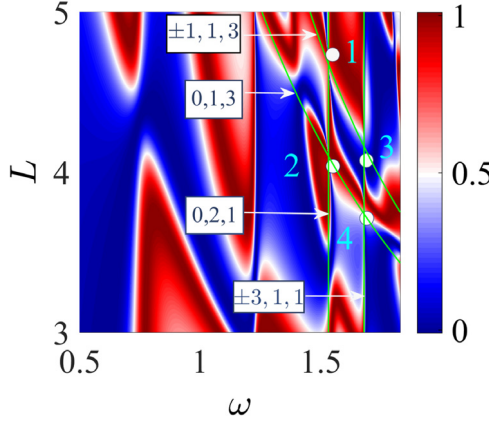


Fig. 3. Transmittance of a cylindrical resonator with radius $R = 2.5$ for the case of non-axisymmetrically attached cylindrical waveguides of unit radius vs. frequency and length of the resonator L . Both waveguides are shifted relative to central axis of the resonator by a distance $r_0 = 1.1$ but have $\Delta\phi = 0$. The solid green lines show the eigenfrequencies of the closed resonator with corresponding indexes mnl . The positions of four BICs are shown by closed white circles. (For interpretation of the references to color in this figure legend, the reader is referred to the web version of this article.)

The S-matrix (13) shows that for transmission of wave with the azimuthal index p there is no scattering into other channels $p' \neq p$ for coaxial case.

For the non axisymmetrically attached waveguides as shown in Fig. 1(b) the S-matrix is not diagonal in the azimuthal index p that substantially increases the computational costs. The advantage of the effective Hamiltonian approach compared to other numerical methods (finite difference methods, the mode-matching techniques *etc.*) is that we can truncate the matrix $\hat{\mathcal{H}}_{\text{eff}}$ retaining only those eigenmodes whose eigenfrequencies are close to the frequency of incident wave (resonant approximation) [14,19].

2. BICs with orbital angular momentum

In what follows we restrict ourselves to the case of the first open channel $p = 0, q = 1$ in the frequency domain $1.8412 > \omega > 0$ where the propagating wave in waveguide is independent of r and ϕ as shown in Table 1. We take the following specific parameters of the axysymmetric open cylindrical resonator: the radius $R = 2.5$, the waveguide shift relative to the resonator axis $r_0 = 1.1$ while the length L is varied. All these quantities are measured in terms of the waveguide radius. Fig. 3 shows the transmittance of circular resonator calculated via Eq. (12) given by $|S_{01L;01R}|^2$. In Fig. 4 we present the scattering function calculated through the Lippmann–Schwinger equation [14,20]

$$\begin{aligned} \psi_L(r', \phi', z) &= \frac{1}{\sqrt{4\pi k_{01}}} [e^{ik_{01}z} \phi_{10} + \sum_{pq} S_{01L;pqL} e^{-ik_{pq}z} \phi_{pq}(r', \phi')], \quad z < 0, \\ \psi_{mnl}(r, \phi, z) &= -i \sum_{m'n'l'} G_{mnl;m'n'l'} \sqrt{\frac{k_p}{\pi}} W_{m'n'l';01}^L, \quad 0 < z < L, \\ \psi_R(r', \phi', z) &= \frac{1}{\sqrt{4\pi k_{01}}} \sum_{pq} S_{01L;pqR} e^{ik_{pq}z} \phi_{pq}(r', \phi'), \quad z > L. \end{aligned} \quad (14)$$

Only the real part of the function which is shown in the form of the pressure field at the surface of the whole structure.

The complex eigenvalues z_r of the effective Hamiltonian

$$\hat{H}_{\text{eff}} \psi_r(r, \phi, z) = z_r \psi_r(r, \phi, z) \quad (15)$$

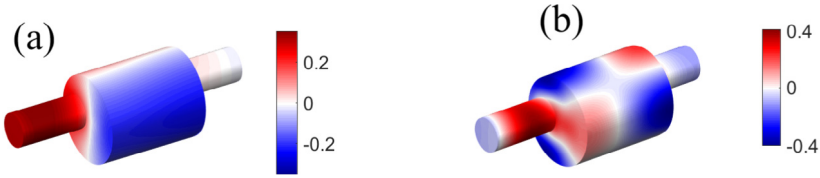


Fig. 4. (Color online) Real part of scattering wave for $\omega = 0.7$ (a) and $\omega = 1.5$ (b). The length of resonator $L = 3$.

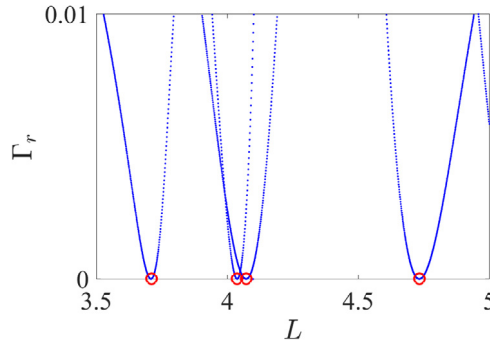


Fig. 5. (Color online) Evolution of resonant widths under variation of the resonator length.

correspond to the positions and widths of the resonant modes $\psi_r(r, \phi, z)$ [17]. The case $Im(z_{BIC}) = 0$ defines a BIC mode with zero resonant width and frequency $\omega_{BIC}^2 = z_{BIC}$ [8]. The results of numerical calculation of the resonant widths as dependent on the resonator length L are presented in Fig. 5. There are four events of the resonant width turning to zero marked by red open circles. They correspond to four BICs listed in Table 1 and shown in Fig. 3 by closed white circles. As was discussed in the Introduction the BICs are the result of accidental degeneracy of the eigenmodes of the same symmetry. There are a few features worthy to discuss. (i) One can see from Fig. 3 that the BIC points are slightly shifted from the degeneracy points because of the contribution of the evanescent modes to the effective Hamiltonian (9) [12]. These evanescent modes contribute into the Hermitian resonator Hamiltonian \hat{H}_R to modify as follows

$$\hat{\mathcal{H}}_R = \hat{H}_R + \sum_{C=L,R} \sum_{p>0,q} k_{pq} \hat{W}_{C,pq} \hat{W}_{C,pq}^+ \quad (16)$$

and respectively shift the points of degeneracy of the modified Hamiltonian $\hat{\mathcal{H}}_R$. (ii) Among the eigenfrequencies there are eigenfrequencies independent of L . As a result we obtain pairs of the BICs with the eigenfrequencies close to each other as presented in Table 2 and seen from Fig. 3. (iii) The modal expansion of the BICs has a property $a_{m,n,l} = a_{-m,n,l}$ resulting in the angular dependence of the BICs in the form $\cos m\phi$ as seen from the patterns in Fig. 6 and modal expansion coefficients in Fig. 7. (iv) Besides the Fridrich–Wintgen BSCs there are numerous symmetry protected odd BICs $\psi_{mn}(r)\psi_l(z)\sin m\phi$ which have zero overlapping integral with the first propagating channel $p = 0, q = 1$ according to Table 1.

3. Spinning BICs

In previous section we considered the BICs for the case when both waveguides were attached to the cylindrical resonator in a non-axisymmetric way as shown in Fig. 1(b) with $\Delta\phi = 0$. That makes the effect of both waveguides identical and summation over $C = L, R$ in the effective Hamiltonian (9)

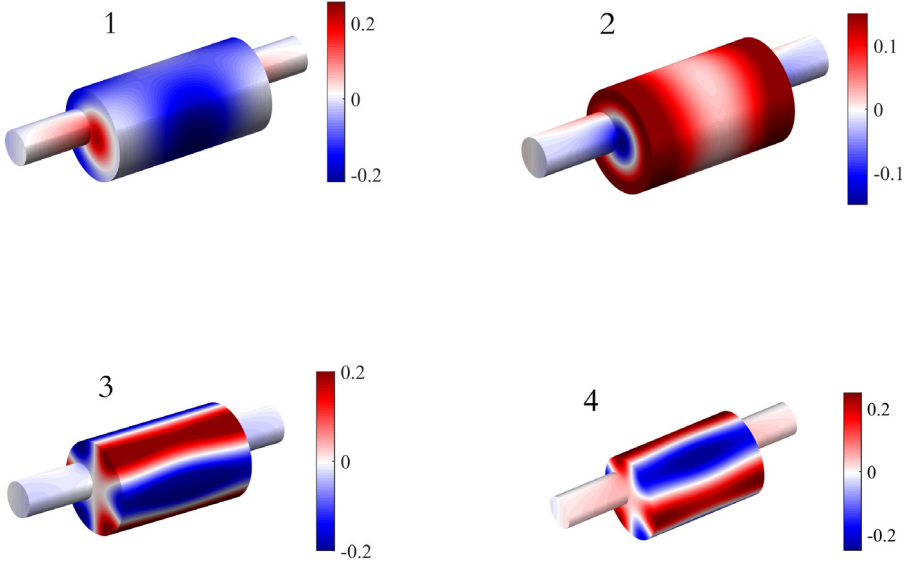


Fig. 6. (Color online) Patterns of BICs from Table 2.

Table 2

Parameters of the BICs for $\Delta\phi = 0$.

BIC number	ω	L	m	n	l
1	1.5506	4.733	0	2	1
			± 1	1	3
2	1.5522	4.037	0	2	1
			0	1	3
3	1.6895	4.072	± 3	1	1
			± 1	1	3
4	1.691	3.7115	± 3	1	1
			0	1	3

simply gives rise to a factor of 2. Let us now attach the waveguides in a non-coaxial way with azimuthal angle difference $\Delta\phi$ as shown in Fig. 1(c). Then the coupling matrices (10) become dependent on the waveguide, either left or right. Because both waveguides are shifted relative to the axis of the resonator by the same distance r_0 as shown in Fig. 8 there is exact relation between the coupling matrix elements

$$W_{mnl;01}^L = W_{mnl}, \quad W_{mnl;01}^R = (-1)^{l-1} e^{im\Delta\phi} W_{mnl} \tag{17}$$

that results in the effective Hamiltonian

$$\langle mnl | \hat{\mathcal{H}}_{\text{eff}} | m' n' l' \rangle = \omega_{mnl}^2 \delta_{mm'} \delta_{nn'} \delta_{ll'} - ik_{01} [1 + (-1)^{l+l'} e^{i(m-m')\Delta\phi}] W_{mnl}^L W_{m'n'l'}^{L*}. \tag{18}$$

The transmittance is shown in Fig. 9. Fig. 10(a) shows the scattering function (14) that demonstrates effect of twisted acoustic pressure field given by real part of ψ . This figure is complemented with quiver plots of the acoustic intensity vector (3) in Fig. 10(b).

In the present paper we consider the case $\Delta\phi = \pi/2$ as shown in Fig. 8. Numerical solution of Eq. (15) reveals multiple BICs as shown in Fig. 11. Corresponding BICs embedded into the first channel $0 < \omega < 1.84118$ are listed in Table 3 and shown by closed white circles in Fig. 9. Surprisingly, the number of the BICs increased compared to the former case of axisymmetric waveguide with $\Delta\phi = 0$. Some patterns of the most interesting BICs are presented in Fig. 12.

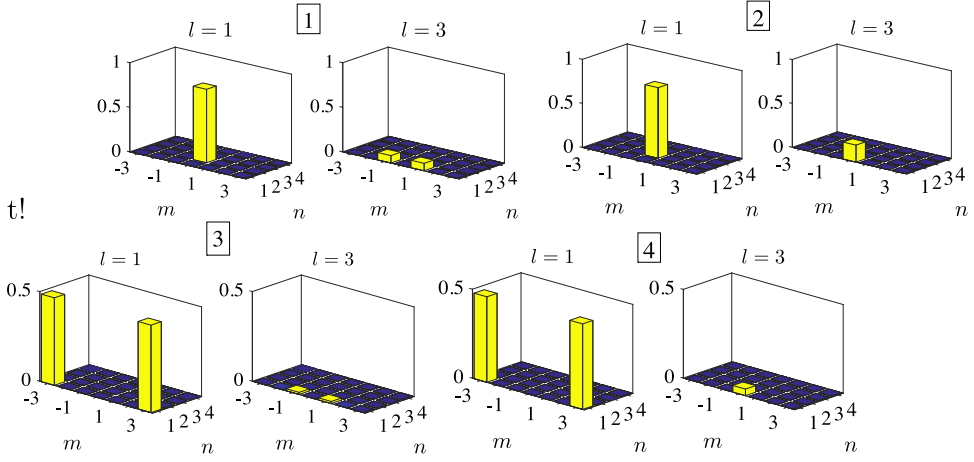


Fig. 7. (Color online) Modal expansion coefficients $|a_{mnl}|$ of BICs shown in Fig. 5 for the case $\Delta\phi = 0$.

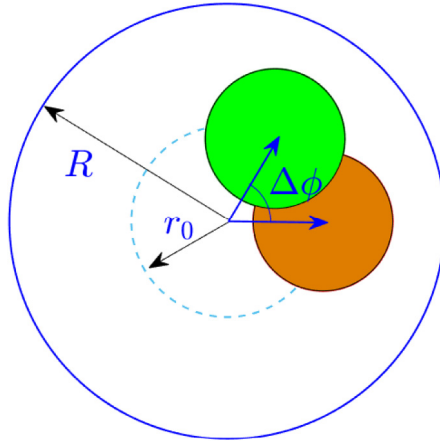


Fig. 8. (Color online) Waveguides attached with azimuthal angles difference $\Delta\phi$.

Let us expand the BICs over the eigenmodes of the closed resonator

$$\psi_{BIC}(r, \phi, z) = \sum_{mnl} a_{mnl} \psi_{mnl}(r, \phi, z) \tag{19}$$

and substitute into Eq. (15). Neglecting the evanescent modes we obtain the following equation for the BIC

$$(\omega_{mnl}^2 - \omega_{BIC}^2) a_{mnl} = ik_{10} W_{mnl} \sum_{m'n'l'} [1 + (-1)^{l+l'} e^{i(m-m')\Delta\phi}] a_{m'n'l'} W_{m'n'l'}^*. \tag{20}$$

Introducing $b_{mnl} = a_{mnl} W_{mnl}^*$ we rewrite this equation as follows

$$(\omega_{mnl}^2 - \omega_{BIC}^2) b_{mnl} = ik_{10} |W_{mnl}|^2 \sum_{m'n'l'} [1 + (-1)^{l+l'} e^{i(m-m')\Delta\phi}] b_{m'n'l'}. \tag{21}$$

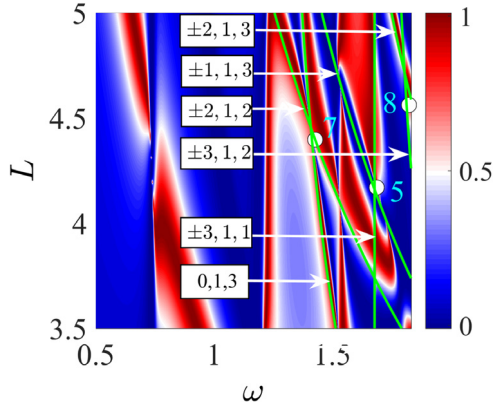


Fig. 9. Transmittance of a cylindrical resonator with radius $R = 2.5$ vs. frequency and length of the resonator. Both waveguides are shifted relative to central axis of the resonator by a distance $r_0 = 1.1$ and have $\Delta\phi = \pi/2$. The solid green lines show eigenfrequencies of closed resonator with corresponding indexes mnl . The positions of the BICs are shown by closed white circles. (For interpretation of the references to color in this figure legend, the reader is referred to the web version of this article.)

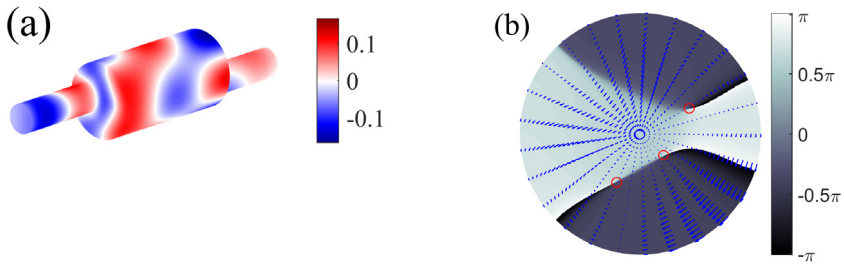


Fig. 10. (a) Real part of scattering function for $\omega = 1.83$ and $L = 4.56$. (b) Phase of the scattering function shown in gray and acoustic intensity vector at $z = L/2$. Open red circles mark points where the phase singularities (phase dislocations) cross the plane $z = L/2$. (For interpretation of the references to color in this figure legend, the reader is referred to the web version of this article.)

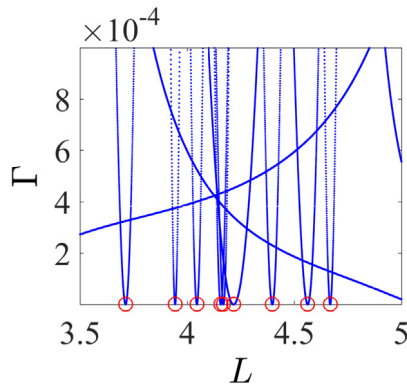


Fig. 11. (Color online) Evolution of resonant widths and resonant frequencies under variation of the resonator length with shifted waveguides.

Table 3
Parameters of BICs for $\Delta\phi = \pi/2$.

BIC number	ω	L	m	n	l
1	1.6907	3.7126	± 3	1	1
			0	1	3
2	1.76	3.944	± 1	1	3
			0	2	2
3	1.5523	4.0454	0	2	1
			0	1	3
4	1.6894	4.157	± 1	1	3
			± 3	1	1
5	1.6894	4.1692	± 1	1	3
			± 3	1	1
6	0.748	4.2166	0	1	3
			± 1	1	1
7	1.4293	4.3972	0	1	3
			± 2	1	2
8	1.826	4.5624	± 2	1	3
			± 3	1	2
9	1.5526	4.6674	0	2	1
			± 1	1	3

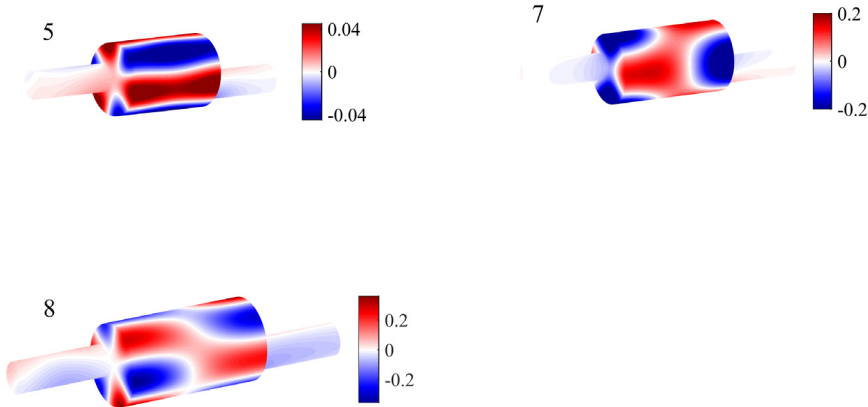


Fig. 12. (Color online) Patterns of the BICs from Table 3.

The solution of Eq. (20) shows that only those eigenmodes of the closed resonator participate in the BICs which undergo the degeneracy under variation of the length L of the resonator in full correspondence with the FW scenario. The only difference with the standard FW theory is that each eigenmode is degenerate in OAM $\pm m$ with the exception of BIC 7 which is formed by one double degenerate eigenmode ± 2 , 1, 2 and one non degenerate eigenmode 0, 1, 3 as shown in Fig. 7. Let us consider some interesting BICs in more detail.

3.1. BIC 5

Let us consider BIC 5 which is formed by four eigenmodes ± 1 , 1, 3 and ± 3 , 1, 1 as shown in Fig. 7. We have from Eq. (21)

$$\begin{aligned}
 (\omega_{113}^2 - \omega_{BIC}^2)b_{113} &= 2ik_{10}|W_{113}|^2(b_{113} + b_{-311}), \\
 (\omega_{311}^2 - \omega_{BIC}^2)b_{-311} &= 2ik_{10}|W_{311}|^2(b_{113} + b_{-311}), \\
 (\omega_{311}^2 - \omega_{BIC}^2)b_{311} &= 2ik_{10}|W_{311}|^2(b_{311} + b_{-113}),
 \end{aligned}$$

Table 4
Modal expansion coefficients of BIC 5 from Table 3.

a_{mnl}	m	n	l
0.688	-3	1	1
-0.163	3	1	1
0.136 - 0.09i	-1	1	3
0.163	1	1	3

$$(\omega_{113}^2 - \omega_{BIC}^2)b_{-113} = 2ik_{10}|W_{113}|^2(b_{311} + b_{-113}). \tag{22}$$

Here we took into account that the coupling matrix elements (10) are real and $W_{-mnl} = W_{mnl}$. Eqs. (22) are easily solved to give

$$b_{113} + b_{-311} = 0, \quad b_{311} + b_{-113} = 0 \tag{23}$$

and correspondingly the BIC frequency $\omega_{BIC} = \omega_{113} = \omega_{311}$. Substituting here the eigenfrequencies (8) we obtain for BIC 5

$$\omega_{BIC} = \frac{\mu_{31}}{R} = 1.68, \quad L_c = \frac{2\pi R}{\sqrt{\mu_{31}^2 - \mu_{11}^2}} = 4.16, \tag{24}$$

where the numerical values of μ_{mn} are listed in Table 1. Comparison with numerical data listed in Table 3 shows a rather good agreement. Eq. (23) predicts for the modal expansion coefficients

$$a_{311}W_{311} = -a_{-113}W_{113}, \quad a_{-311}W_{311} = -a_{113}W_{-113}, \tag{25}$$

Numerical evaluation of the coupling matrix elements $W_{mnl;01}$ (10) gives us the following values for $W_{113} = 0.403$, $W_{311} = 0.174$ and respectively according to Eq. (25) we obtain $a_{311}/a_{-113} = a_{-311}/a_{113} = -W_{113}/W_{311} = 4$. These relations are also close to numerical results in Table 3 obtained with the use of the effective Hamiltonian (9) expanded onto 2016 eigenmodes and with account of 71 evanescent modes (see Table 4).

Eq. (25) shows that at the point (24) we have two degenerate BICs which according to Eq. (19) can be presented

$$\begin{aligned} \psi_{BIC,1}(r, \phi, z) &\approx W_{311}\psi_{11}(r)\psi_3(z)e^{-i\phi} - W_{311}\psi_{31}(r)\psi_1(z)e^{3i\phi}, \\ \psi_{BIC,2}(r, \phi, z) &\approx W_{311}\psi_{11}(r)\psi_3(z)e^{i\phi} - W_{311}\psi_{31}(r)\psi_1(z)e^{-3i\phi}. \end{aligned} \tag{26}$$

The degeneracy of BIC 5 is related to the symmetry of the closed resonator relative to $\phi \rightarrow -\phi$ as seen from Eq. (19). As the BIC point is approached in the parametric space the BIC solution dominates in the scattering function

$$\psi \approx \sum_{r=1,2} \alpha_r \psi_{BSC,r}(r, \phi, z). \tag{27}$$

where the superposition coefficients tend to infinity and extremely sensitive to the way of approach [12]. This phenomenon constitutes the important effect of enhancement of the injected sound within the resonator [12,21,22]. More interesting is that the scattering function (27) carries vortical acoustic intensity (3) as demonstrated in Fig. 13. The intensity vector follows $\nabla \arg(\psi)$ according to Eq. (3). The phase of the scattering function $\arg(\psi)/\pi$ is shown by gray scale in Fig. 13(a) for $z = L/2$.

3.2. BIC 7

BIC 7 is given by two degenerate eigenmodes $\pm 2, 1, 2$ and single eigenmode 0, 1, 3. This BIC is interesting since one of linear combinations of degenerate modes forms function $J_2(\mu_{21}r)\psi_2(z) \sin 2\phi$

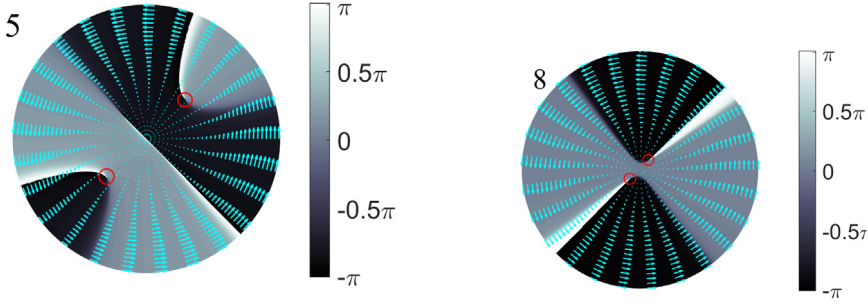


Fig. 13. (Color online) Phase of the scattering function and acoustic intensity at $z = L/2$ in the close vicinity to BICs 5 and 8.

Table 5
Modal expansion coefficients of BIC 7 from Table 3.

a_{mnl}	m	n	l
0.5929	-2	1	2
0.5929	2	1	2
-0.537	0	1	3

which has zero coupling with both waveguides shifted by angle $\Delta\phi = \pi/2$ and therefore is a symmetry protected BIC. Then the other two modes

$$\psi_1 = J_2(\mu_{21}r)\psi_2(z) \cos 2\phi, \quad \psi_2 = J_0(\mu_{01}\psi_3(z)) \tag{28}$$

become degenerate with variation of the resonator length L to yield

$$L_c = \frac{\sqrt{3}\pi R}{\mu_{21}} = 4.46, \quad \omega_{BIC} = \frac{2\pi}{L_c} = 1.41. \tag{29}$$

This is also close to the numerical data in Table 3. Approximating BIC 7 mode by superposition

$$\psi_{BIC} \approx a_{212} \frac{\psi_{212} + \psi_{-212}}{\sqrt{2}} + a_{013} \psi_{013}$$

we obtain from Eq. (21)

$$\begin{aligned} (\omega_{212}^2 - \omega_{BIC}^2)b_{212} &= 2ik_{10}|W_{212}|^2(2b_{212} + b_{013}), \\ (\omega_{013}^2 - \omega_{BIC}^2)b_{013} &= 2ik_{10}|W_{013}|^2(b_{013} + 4b_{212}). \end{aligned} \tag{30}$$

This equation gives for the modal expansion coefficients

$$2a_{212}W_{212} = -a_{013}W_{013} \tag{31}$$

Numerical evaluation of the coupling matrix elements (10) gives us the following values for $W_{212} = 0.117$, $W_{013} = 0.27$ and subsequently according to Eq. (25) $a_{212}/a_{013} = -1.154$. This ratio is also close to numerical results in Table 5.

3.3. BIC 8

BIC 8 is given by a pair of double degenerate eigenmodes $\pm 2, 1, 3$, and modes $\pm 3, 1, 2$. The first two degenerate modes forms function

$$J_2(\mu_{21}r)\psi_3(z) \sin 2\phi$$

Table 6
Modal expansion coefficients of BIC 8 from Table 3.

a_{mnl}	m	n	l
0.671	−3	1	2
−0.671i	3	1	2
−0.128 + 0.18i	−2	1	3
−0.128 + 0.18i	2	1	3

which has zero coupling with both waveguides shifted by angle $\Delta\phi = \pi/2$ and therefore is a symmetry protected BIC. Then the other three eigenmodes

$$J_2(\mu_{21}r)\psi_3(z)\cos 2\phi, \quad \psi_{\pm 312}(r, \phi, z) \quad (32)$$

become degenerate for variation L to yield

$$L_c = \frac{\sqrt{3}\pi R}{\sqrt{\mu_{31}^2 - \mu_{21}^2}} = 4.71, \quad \omega_{BIC} = 1.81, \quad (33)$$

which again is a good agreement with the numerical data in Table 3. The BIC 8 shape function mode is given

$$\psi_{BIC} \approx a_{213} \frac{\psi_{213} + \psi_{-213}}{\sqrt{2}} + a_{312}\psi_{312} + a_{-312}\psi_{-312}$$

. From Eq. (21) we have

$$\begin{aligned} (\omega_{213}^2 - \omega_{BIC}^2)b_{213} &= ik_{10}|W_{213}|^2[4b_{213} + (1+i)b_{312} + (1-i)b_{-312}], \\ (\omega_{312}^2 - \omega_{BIC}^2)b_{312} &= 2ik_{10}|W_{312}|^2[(1-i)b_{213} + b_{312}], \\ (\omega_{312}^2 - \omega_{BIC}^2)b_{-312} &= 2ik_{10}|W_{312}|^2[(1+i)b_{213} + b_{-312}]. \end{aligned} \quad (34)$$

At the BIC point these equations give $\omega_{BIC} = \omega_{213} = \omega_{312}$ and the following solution for BIC 8:

$$W_{312}a_{312} = -(1-i)W_{213}a_{213}, \quad W_{312}a_{-312} = -(1+i)W_{213}a_{213}, \quad a_{-312} = ia_{312}. \quad (35)$$

The numerical results in Table 6 deviate from Eqs. (35) for the frequency of BIC 8 frequency 1.81 is close to the next propagating band at 1.84 where the contribution of the evanescent modes is important.

4. Conclusions

We considered acoustic trapped modes or bound states in the continuum in a non-axisymmetric duct-cavity structure which consists of a cylindrical resonator and two cylindrical waveguides whose axes are shifted relative to the axis of the resonator by a distance r_0 . Moreover the axes of the waveguides can be shifted relative to each other by azimuthal angle $\Delta\phi$ as shown in Fig. 1(c) and 8. The way of attachment does not change the eigenfrequencies of the closed resonator but changes the effective non-Hermitian Hamiltonian. The eigenvalue spectrum of the resonator can be rearranged in a realistic acoustic experiment by the use of piston-like hollow-stem waveguides tightly fit to the interior boundaries of a cylindrical cavity [8].

Even in the simplest case $r_0 \neq 0$, $\Delta\phi = 0$ two cases the orbital angular momentum (OAM) m is not preserved because of the lack of rotational symmetry. In that case we found multiple BICs with nonzero OAM under variation of the resonator length L which differ from the BICs with zero OAM found in the axisymmetric cylindrical waveguide [8]. Irrespectively to the choice of r_0 the BICs occur at the points of degeneracy of two eigenmodes of the same symmetry of the closed cylindrical resonator. That mechanism of wave localization was first described by [11] and has been so far experimentally realized only in microwave set-ups [23,24].

Far more rich variety of the BICs is observed in the case when the axes of the waveguides are shifted relative to each other by azimuthal angle $\Delta\phi$. The two resonance FW scenario is replaced by

interference of three or four resonant modes with to form two degenerate complex BICs related to each other by complex conjugation. Respectively the BICs carry the intensity vectors with opposite direction. Independently of the choice of $\Delta\phi$ or r_0 the injected wave with zero orbital angular momentum $m = 0$ transmits and reflects with same OAM when only the first channel is opened for the frequency $\omega < 1.841$. However the case $\Delta\phi \neq 0$ is of special interest because of formation of spiraling flows of acoustic intensity inside the resonator. In this case the chirality of the system lifts the degeneracy of the resonant modes with respect to the sign of orbital angular momentum. The spiraling acoustic intensity enhances enormously in the vicinity of the BIC points. This enhancement can be controlled by simultaneous variation of the length of the resonator and rotation of one of the waveguides. Presently a programmable spatial light modulator comprising a system of lenses, grating, or phase-diffracting elements has been used to produce the spiraling acoustic beams [25–28]. The present approach which exploits the acoustic BICs provides promising tool to generate orbital angular momentum in acoustic.

Acknowledgments

This work has been supported by RFBR Grant 17-02-00440. We thank D.N. Maksimov for discussions.

References

- [1] F. Urcell, *Math. Proc. Cambridge Philos. Soc.* 47 (1951) 347–358.
- [2] F. Urcell, *Proc. R. Soc. Lond. Ser. A Math. Phys. Eng. Sci.* 435 (1991) 575–589.
- [3] C.M. Linton, P. McIver, *Jl Mech. Appl. Math.* 51 (1998) 389–412.
- [4] M. Callan, C.M. Linton, D.V. Evans, *J. Fluid Mech.* 229 (1991) 51–64.
- [5] D.V. Evans, R. Porter, *J. Fluid Mech.* 339 (1997) 331–356.
- [6] T. Utsunomiya, R.E. Taylor, *J. Fluid Mech.* 386 (1999) 259–279.
- [7] S. Hein, W. Koch, L. Nannen, *J. Fluid Mech.* 692 (2012) 257–287.
- [8] A.A. Lyapina, D.N. Maksimov, A.S. Pilipchuk, A.F. Sadreev, *J. Fluid Mech.* 780 (2015) 370–387.
- [9] L. Xiong, W. Bi, Y. Aurégan, *J. Acoust. Soc. Am.* 139 (2016) 764–772.
- [10] S. Hein, W. Koch, *J. Fluid Mech.* 605 (2008) 401–428.
- [11] H. Friedrich, D. Wintgen, *Phys. Rev. A* 32 (1985) 3231.
- [12] A.F. Sadreev, E.N. Bulgakov, I. Rotter, *Phys. Rev. B* 73 (2006) 235342.
- [13] D.M.F. Chapman, *J. Acoust. Soc. Am.* 124 (2008) 48–56.
- [14] D.N. Maksimov, A.F. Sadreev, A.A. Lyapina, A.S. Pilipchuk, *Wave Motion* 56 (2015) 52–79.
- [15] H. Feshbach, *Ann. Phys., NY* 5 (1958) 357–390.
- [16] H. Feshbach, *Ann. Phys., NY* 19 (1962) 287–313.
- [17] J. Okołowicz, M. Płoszajczak, I. Rotter, *Phys. Rep.* 374 (2003) 271–383.
- [18] F.M. Dittes, *Phys. Rep.* 339 (2000) 215–316.
- [19] K. Pichugin, H. Schanz, P. Seba, *Phys. Rev. E* 64 (2001) 056227.
- [20] A.F. Sadreev, I. Rotter, *J. Phys. A: Math. Gen.* 36 (2003) 11413–11433.
- [21] Mingda Zhang, Xiangdong Zhang, *Sci. Rep.* 5 (2015) 8266, 1–7.
- [22] Maowen Song, Honglin Yu, Changtao Wang, Na Yao, Mingbo Pu, Jun Luo, Zuojun Zhang, Xiangang Luo, *Opt. Express* 23 (2015) 2895–2903.
- [23] T. Lepetit, E. Akmansoy, J.-P. Ganne, J.-M. Lourtioz, *Phys. Rev. B* 82 (2010) 195307.
- [24] T. Lepetit, B. Kante, *Phys. Rev. B* 90 (2014) 241103(R).
- [25] B.T. Hefnera, P.L. Marston, *J. Acoust. Soc. Am.* 106 (1999) 3313–3316.
- [26] J.L. Ealo, J.C. Prieto, F. Seco, *IEEE Trans. Ultrason. Ferroelectr. Freq. Control* 58 (2011) 1651–1657.
- [27] Zhen Yu Hong, Jie Zhang, B.W. Drinkwater, *Phys. Rev. Lett.* 114 (2015) 214301.
- [28] Xue Jiang, Yong Li, Bin Liang, Jian-chun Cheng, Likun Zhang, *Phys. Rev. Lett.* 117 (2016) 034301.